J|A|C|S
ARTICLES

Highly Disordered Polymer Field Effect Transistors: *N*-Alkyl Dithieno[3,2-*b*:2′,3′-*d*]pyrrole-Based Copolymers with Surprisingly High Charge Carrier Mobilities

Junying Liu, Rui Zhang, Geneviève Sauvé, Tomasz Kowalewski, and Richard D. McCullough*

Department of Chemistry, Carnegie Mellon University, 4400 Fifth Avenue, Pittsburgh, Pennsylvania 15213

Received May 9, 2008; E-mail: rm5g@andrew.cmu.edu

Abstract: A series of novel electroactive and photoactive conjugated copolymers based on *N*-alkyl dithieno[3,2-*b*:2′,3′-*d*]pyrroles (DTP) and thiophene (TH) units (DTP-*co*-THs) were synthesized using a Stille coupling reaction and exhibited molecular weights of 1.6×10^4 to 5.0×10^4 g/mol. The incorporation of soluble substituted thiophenes and planar DTP units resulted in low band gap, highly conductive polymers. DTP-*co*-THs exhibited excellent solubility in common organic solvents and formed high-quality films. Optical characterization revealed that the band gaps of DTP-*co*-THs were between 1.74 and 2.00 eV, lower than regioregular poly(3-alkylthiophenes). Electrochemical characterization showed that the HOMO energy levels of DTP-*co*-THs are between −4.68 and −4.96 eV. When doped, DTP-*co*-THs exhibited high conductivities up to 230 S/cm with excellent stability. The different thiophene substituent patterns' effect on the polymers' optical and electronic properties was then examined by density functional theory computations. The microstructure and surface morphologies of poly(2,6-(4-dodecyl-4*H*-bisthieno[3,2-*b*:2′,3′-*d*]pyrrole)-random-2,5-(3-dodecylthiophene)) (P4) and poly(2-(4,4′-didodecyl-2,2′-bithiophen-5-yl)-4-octyl-4*H*-bisthieno[3,2-*b*:2′,3′-*d*]pyrrole) (P6) thin films were studied by X-ray diffraction and atomic force microscopy. As-cast P4 and P6 thin films exhibited poorly defined, randomly ordered lamellar structure that improved significantly after thermal annealing. Field effect transistor devices fabricated from P4 and P6 showed typical p-channel transistor behavior. Interestingly, the mobilities of as-cast, less ordered samples were much higher than those observed after annealing. The highest values of maximum and average mobilities were observed for the polymer P6 as-cast (0.21 and 0.13 $cm^2\ V^{-1}\ s^{-1}$, respectively). One of our goals was to test the idea that high mobility and excellent electrical and structural reproducibility could perhaps be achieved by the creation of amorphous π-conjugated materials that could possess long arrange π connectivity on the microscopic scale. The results of these studies strongly suggest that the presence of highly ordered microcrystalline structures in thin films of organic semiconductors is not necessary for excellent performance of organic transistors.

Introduction

Conjugated polymers have received considerable attention, since they can be processed in simpler and more cost-effective ways than their inorganic counterparts.[1,2] Another advantage of these materials is that they can be molecularly engineered to have tunable electronic and optical properties.[2] The key to this molecular engineering is the ability to control the dimensional π conjugation and connectivity essentially through synthesis and assembly.[3]

There are multiple strategies for tuning π conjugation, and three of these strategies are described below. One strategy is the synthesis of regioregular polymers, such as regioregular poly(3-alkylthiophenes) (*rr*-P3ATs), which generates defect-free,[3,4] structurally homogeneous head-to-tail (HT) coupling, leading to enhanced π conjugation, well-defined supermolecular structure, and greatly improved electronic and optical properties. A second strategy is the synthesis of an alternative donor−acceptor system.[5] The third approach is the introduction of fused aromatic rings into the conjugated polymer backbone, which has been

(1) (a) Garnier, F.; Hajlaoui, R.; Yassar, A.; Srivastava, P. *Science* **1994**, *265*, 1684. (b) Sirringhaus, H.; Tessler, N.; Friend, R. H. *Science* **1998**, *280*, 1741. (c) Ong, B. S.; Wu, Y.; Liu, P.; Gardner, S. *J. Am. Chem. Soc.* **2004**, *126*, 3378.

(2) (a) Bao, Z.; Rogers, J. A.; Katz, H. E. *J. Mater. Chem.* **1999**, *9*, 1895. (b) Locklin, J.; Li, D.; Mannsfeld, S.; Borkent, E.; Meng, H.; Advincula, R.; Bao, Z. *Chem. Mater.* **2005**, *17*, 3366.

(3) McCullough, R. D.; Lowe, R. D.; Jayaraman, M.; Anderson, D. L. *J. Org. Chem.* **1993**, *58*, 904.

(4) (a) McCullough, R. D.; Lowe, R. D. *J. Chem. Soc., Chem. Commun.* **1992**, *1*, 70. (b) Bjφrnholm, T.; Greve, D. R.; Reitzel, N.; Hassenkam, T.; Kjaer, K.; Howes, P. B.; Larsen, N. B.; Bøgelund, J.; Jayaraman, M.; Ewbank, P. C.; McCullough, R. D. *J. Am. Chem. Soc.* **1998**, *120*, 7643. (c) Liu, J.; Sheina, E.; Kowalewski, T.; McCullough, R. D. *Angew. Chem., Int. Ed.* **2002**, *41*, 329.

(5) (a) Karikomi, M.; Kitamura, C.; Tanaka, S.; Yamashita, Y. *J. Am. Chem. Soc.* **1995**, *117*, 6791. (b) Lee, B.; Yamamoto, T. *Macromolecules* **1999**, *32*, 1375. (c) Jenekhe, S. A.; Lu, L.; Alam, M. M. *Macromolecules* **2001**, *34*, 7315. (d) Zhu, Y.; Champion, R. D.; Jenekhe, S. A. *Macromolecules* **2006**, *39*, 8712. (e) Osaka, I.; Sauvé, G.; Zhang, R.; Kowalewski, T.; McCullough, R. D. *Adv. Mater.* **2007**, *19*, 4160.

10.1021/ja803077v CCC: $40.75
Published on Web 09/04/2008

used to achieve polymers with high charge carrier mobility.[6] The incorporation of fused rings can lead to a more rigid and planar polymer backbone, thereby enhancing effective π conjugation, preventing chain-folding, and lowering the band gap. Furthermore, the rigid fused ring structure can lower the reorganization energy of the molecule, facilitating intermolecular hopping and charge carrier mobility.[7,8] Various aromatic fused ring-based conjugated polymers have been developed for their use in potential applications, such as organic light-emitting diodes (OLEDs),[9,10] organic photovoltaic devices (OPVs),[11−13] and field effect transistors (FETs).[14] In particular, FET performance can be greatly improved by incorporating thiophene-based fused rings into polymers, such as thienothiophene,[6] benzodithiophene,[15] and cyclopentadithiophene.[14a]

Rasmussen and co-workers pioneered the use of *N*-alkyl dithieno[3,2-*b*:2′,3′-*d*]pyrrole (DTP) as a very promising fused aromatic building block for electronic materials.[16] It has a completely flat crystal structure, indicating good π conjugation across the fused rings. Upon polymerization, poly(*N*-alkyl dithieno[3,2-*b*:2′,3′-*d*]pyrroles) (PDTPs) exhibit excellent stability in their oxidized state, have low band gaps, and show efficient red fluorescence in solution.[17] However, some PDTPs have low solubilities and low molecular weight, which greatly limits their use in devices. To improve the solubility of PDTPs and to create a number of DTP-based copolymers, we incorporated substituted thiophene units into the polymer backbone and generated a series of novel low band gap copolymers with excellent solubility, high molecular weights, and highly interesting electronic properties.

In this article, we describe the synthesis, characterization, electrical conductivity, and field effect mobility of a series of novel soluble *N*-alkyl DTP and thiophene (TH)-based copolymers (DTP-*co*-THs) and compare them to well-studied *rr*-P3HT. Various substituted thiophene units and DTP were incorporated into the polymer backbone to tune the electronic and optical properties. Furthermore, we investigated the effects of the alkyl side chain length on the aromatic rings, the TH/DTP ratios in the polymer backbone, and a variety of coupled bialkylthiophenes on resulting polymer properties. The incorporation of planar DTP units extends π conjugation, and the introduction of thiophene subunits imparts good solubility, high conductivity, and high charge carrier mobility. Therefore, the incorporation of DTP units and various substituted thiophenes into the polymer backbone affords the ability to enhance the solubility, lower the band gap, and achieve the enhanced electronic properties. One of our goals was to test the idea that high mobility and excellent electrical and structural reproducibility could perhaps be achieved by creating amorphous π-conjugated materials that could possess long arrange π connectivity on the microscopic scale.[14d,18] Here, we present the results that suggest the presence of highly ordered microcrystalline structures in thin films of polymeric semiconductors is not necessary for excellent performance of organic transistors.

Experimental Section

Materials. 2,5-Dibromo-3-alkylthiophene,[19] 2,5-dibromo-3,4-didodecylthiophene,[20] 5,5′-dibromo-3,3′-dihexyl-2,2′-bithiophene,[21] 5,5′-dibromo-4,4′-bi(dodecyl)-2,2′-bithiophene,[6b] and *N*-alkyl dithieno[3,2-*b*:2′,3′-*d*]pyrroles[22] were prepared according to literature procedures. *N*-Alkyl-2,6-bis(trimethylstannyl)dithieno[3,2-*b*:2′3′-*d*]pyrroles were synthesized according to Scheme 1.

***N*-Dodecyldithieno[3,2-*b*:2′3′-*d*]pyrrole (1b).** This compound was also synthesized by the procedure reported by Samyn and coworkers[22] to give a white solid in 81% yield. ^{1}H NMR (300 MHz, $CDCl_3$, ppm): 7.14 (d, J = 5.4 Hz, 2H), 7.02 (d, J = 5.4 Hz, 2H), 4.21 (t, J = 7.1 Hz, 2H), 1.89 (m, 2H), 1.26 (m, 18H), 0.89 (t, J = 6.9 Hz, 3H). ^{13}C NMR ($CDCl_3$, ppm): 144.96, 122.74, 114.65, 110.94, 47.44, 31.91, 30.36, 29.59, 29.57, 29.55, 29.45, 29.32, 29.24, 26.99, 22.68, 14.11. Elemental Anal. ($C_{20}H_{29}NS_2$) Calcd: C, 69.11; H, 8.41; N, 4.03; S, 18.45. Found: C, 69.45; H, 8.26; N, 4.22; S, 18.06.

***N*-Octyl-2,6-bis(trimethylstannyl)dithieno[3,2-*b*:2′3′-*d*]-pyrrole (2a).** *N*-Octyl dithieno[3,2-*b*:2′,3′-*d*]pyrrole (3.0 mmol, 875 mg) was dissolved in dry THF (200 mL) and cooled to −78 °C under nitrogen. *tert*-Butyllithium (7.5 mmol, 4.4 mL) was then added dropwise. The resulting solution was stirred for 1 h at −78 °C and then slowly warmed to room temperature, followed by

(6) (a) Heeney, M.; Bailey, C.; Genevicius, K.; Shkunov, M.; Sparrowe, D.; Tierney, S.; McCulloch, I. *J. Am. Chem. Soc.* **2005**, *127*, 1078. (b) McCulloch, I.; Heeney, M.; Genevicius, K.; MacDonald, I.; Shkunov, M.; Sparrowe, D.; Tierney, S.; Wagner, R.; Zhang, W.; Chabinyc, M. L.; Kline, R. J.; McGehee, M. D.; Toney, F. M. *Nat. Mater.* **2006**, *5*, 328.

(7) Coppo, P.; Turner, M. L. *J. Mater. Chem.* **2005**, *15*, 1123.

(8) Hutchison, G. R.; Ratner, M. A.; Marks, T. J. *J. Am. Chem. Soc.* **2005**, *127*, 2339.

(9) (a) Scherf, U.; List, E. W. *Adv. Mater.* **2002**, *14*, 477. (b) Woudenbergh, T. V.; Wildeman, J.; Blom, P. M.; Bastiaansen, J. A. M.; Langeveld-Voss, B. W. *Adv. Funct. Mater.* **2004**, *14*, 677. (c) Yu, W. L.; Pei, J.; Huang, W.; Heeger, A. J. *Adv. Mater.* **2000**, *12*, 828. (d) Setayesh, S.; Grimsdale, A. C.; Weil, T.; Enkelmann, V.; Müllen, K.; Meghdadi, F.; List, E. J. W.; Leising, G. *J. Am. Chem. Soc.* **2001**, *123*, 946. (e) Liu, J.; Guo, X.; Bu, L.; Xie, Z.; Cheng, Y.; Geng, Y.; Wang, L.; Jing, X.; Wang, F. *Adv. Funct. Mater.* **2007**, *17*, 1917. (f) Gong, X.; Robinson, M. R.; Ostrowski, J. C.; Moses, D.; Bazan, G. C.; Heeger, A. J. *Adv. Mater.* **2002**, *14*, 581. (g) Lim, E.; Jung, B. J.; Shim, H. K. *Macromolecules* **2003**, *36*, 4288.

(10) Braun, D. *Mater. Today* **2002**, *5*, 32.

(11) (a) Svensson, M.; Zhang, F.; Veenstra, S.; Verhees, W. H.; Hummelen, J.; Kroon, J.; Inganäs, O.; Andersson, M. R. *Adv. Mater.* **2003**, *15*, 988. (b) Mühlbacher, D.; Scharber, M.; Morana, M.; Zhu, Z.; Waller, D.; Gaudiana, R.; Brabec, C. *Adv. Mater.* **2006**, *18*, 2884. (c) Blouin, N.; Michaud, A.; Leclerc, M. *Adv. Mater.* **2007**, *19*, 2295. (d) Soci, C.; Hwang, I.-W.; Moses, D.; Zhu, Z.; Waller, D.; Gaudiana, R.; Brabec, C. J.; Heeger, A. J. *Adv. Funct. Mater.* **2007**, *17*, 632.

(12) (a) Jørgensen, M.; Norrman, K.; Krebs, F. C. *Sol. Energy Mater. Sol. Cells* **2008**, *92*, 686. (b) Günes, S.; Neugebauer, H.; Sariciftci, N. S. *Chem. Rev.* **2007**, *107*, 1324.

(13) (a) Winder, C.; Sariciftci, N. S. *J. Mater. Chem.* **2004**, *14*, 1077. (b) Bundgaard, E.; Krebs, F. C. *Sol. Energy Mater. Sol. Cells* **2007**, *91*, 954.

(14) (a) Zhang, M.; Tsao, H. N.; Pisula, W.; Yang, C.; Mishra, A. K.; Müllen, K. *J. Am. Chem. Soc.* **2007**, *129*, 3472. (b) Usta, H.; Lu, G.; Facchetti, A.; Marks, T. J. *J. Am. Chem. Soc.* **2006**, *128*, 9034. (c) Allard, S.; Forster, M.; Souharce, B.; Thiem, H.; Scherf, U. *Angew. Chem., Int. Ed.* **2008**, *47*, 4070. (d) Sirringhaus, H. *Adv. Mater.* **2005**, *17*, 2411.

(15) Pan, H.; Li, Y.; Wu, Y.; Liu, P.; Ong, B. S.; Zhu, S.; Xu, G. *J. Am. Chem. Soc.* **2007**, *129*, 4112.

(16) (a) Ogawa, K.; Rasmussen, S. C. *J. Org. Chem.* **2003**, *68*, 2921. (b) Ogawa, K.; Stafford, J. A.; Rothstein, S. D.; Tallman, D. E.; Rasmussen, S. C. *Synth. Met.* **2005**, *152*, 137.

(17) (a) Ogawa, K.; Rasmussen, S. C. *Macromolecules* **2006**, *39*, 1771. (b) Koeckelberghs, G.; Samyn, C. *Macromolecules* **2005**, *38*, 4545.

(18) (a) Shirota, Y. *J. Mater. Chem.* **2000**, *10*, 1. (b) Shirota, Y. *J. Mater. Chem.* **2005**, *15*, 75. (c) Shirota, Y.; Kageyama, H. *Chem. Rev.* **2007**, *107*, 953. (d) Veres, J.; Ogier, S. D.; Leeming, S. W.; Cupertino, D. C.; Khaffaf, S. M. *Adv. Funct. Mater.* **2003**, *13*, 199. (e) Veres, J.; Ogier, S. D.; Lloyd, G.; Leeuw, D. D. *Chem. Mater.* **2004**, *16*, 4543. (f) Veres, J.; Ogier, S.; Leeming, S.; Brown, B.; Cupertino, D. C. *Mater. Res. Soc. Symp. Proc.* **2002**, 708.

(19) (a) Loewe, R.; Khersonsky, S.; McCullough, R. D. *Adv. Mater.* **1999**, *11*, 250. (b) Loewe, R. S.; Ewbank, P. C.; Liu, J.; Zhai, L.; McCullough, R. D. *Macromolecules* **2001**, *34*, 4324.

(20) (a) Andreani, F.; Salatelli, E.; Lanzi, M. *Polymer* **1996**, *37*, 661. (b) Liu, B.; Yu, W.; Lai, Y.; Huang, W. *Macromolecules* **2000**, *33*, 8945.

(21) Higuchi, H.; Nakayama, T.; Koyama, H.; Ojima, J.; Wada, T.; Sasabe, H. *Bull. Chem. Soc. Jpn.* **1995**, *68*, 2363.

(22) Koeckelberghs, G.; Cremer, L. D.; Vanormelingen, W.; Dehaen, W.; Verbiest, T.; Persoons, A.; Samyn, C. *Tetrahedron* **2005**, *61*, 687.

Scheme 1. Synthetic Route for Monomers and Polymers

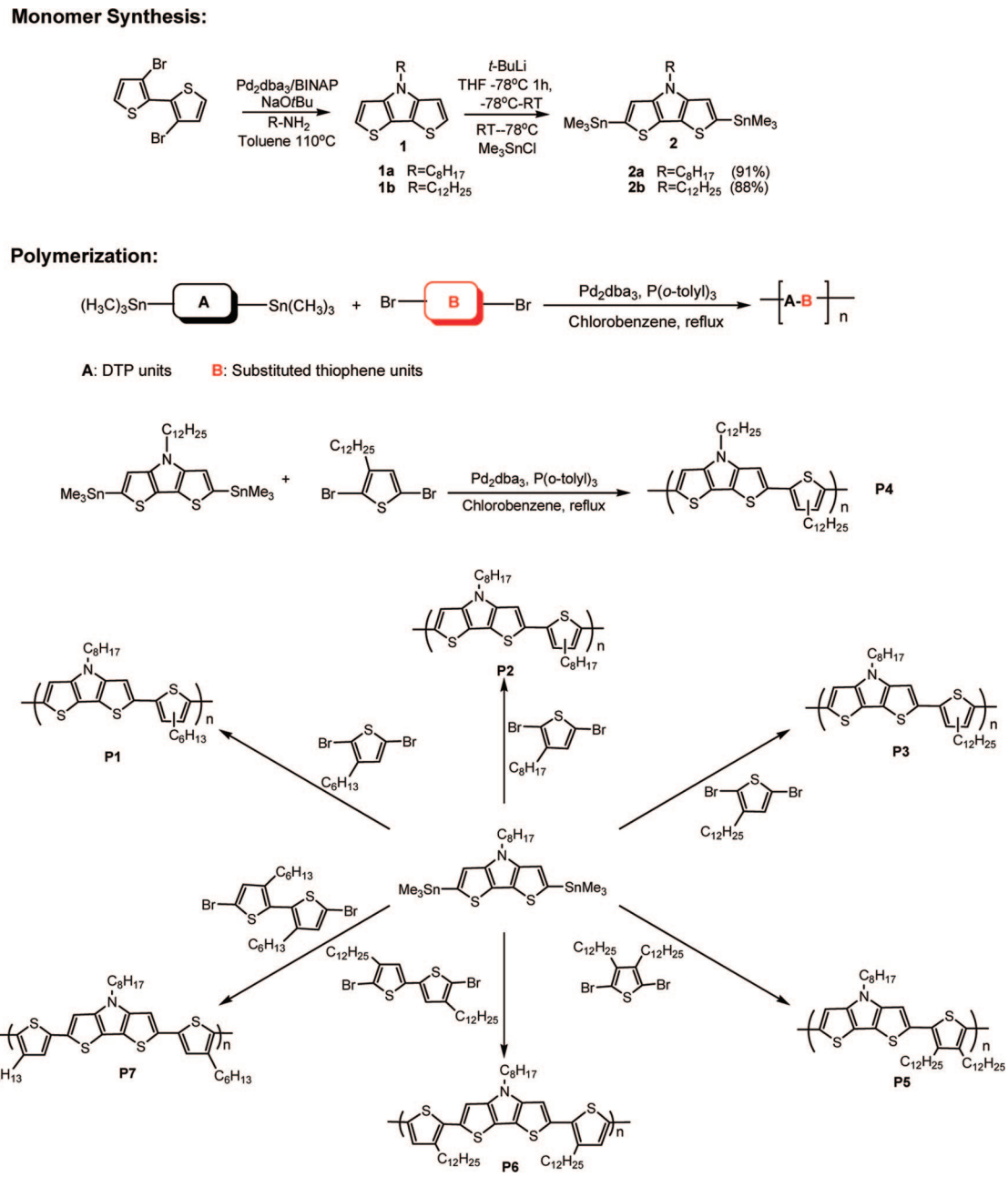

cooling to −78 °C for 15 min. Trimethyltin chloride (7.5 mmol, 7.5 mL) was added in one portion. After addition, the mixture was warmed to room temperature and stirred for another 2 h. The reaction was quenched with water, and the aqueous layer was extracted with diethyl ether. The organics were washed with water and then brine and then dried over anhydrous $MgSO_4$. Removal of the solvent gave the product as brown solid in 91% yield. ^{1}H NMR (300 MHz, $CDCl_3$, ppm): 7.02 (s, 2H), 4.20 (t, J = 7.1 Hz, 2H), 1.90 (m, 2H), 1.28 (m, 10H), 0.89 (t, J = 6.7 Hz, 3H), 0.42 (s, 18H).

***N*-Dodecyl-2,6-bis(trimethylstannyl)dithieno[3,2-*b*:2′3′-*d*]-pyrrole (2b).** The same procedure as above. Light brown solid. Yield: 88%. ^{1}H NMR (300 MHz, $CDCl_3$, ppm): 7.02 (s, 2H), 4.20 (t, J = 7.2 Hz, 2H), 1.90 (m, 2H), 1.28 (m, 18H), 0.90 (t, J = 6.7 Hz, 3H), 0.42 (s, 18H).

Synthesis of Polymers.

General Procedure of Polymerization by Stille Cross-Coupling Reaction. Equimolar amounts of *N*-alkyl-2,6-bis(trimethylstannyl)dithieno[3,2-*b*:2′3′-*d*]pyrrole (0.3 mmol) and dibrominated thiophene derivatives (0.3 mmol) were dissolved in anhydrous chlorobenzene (10 mL) followed by the addition of tris(dibenzylideneacetone)dipalladium(0) (3.0 mol %, 5.49 mg) and tri(*o*-tolyl)phosphine (6.0 mol %, 3.65 mg) under N_2. The resulting mixture was refluxed for 2 days under N_2. After being cooled to room temperature, the reaction was precipitated into a mixture of methanol (100 mL) and concentrated hydrochloric acid (5 mL) and stirred for 2 h at room temperature. The precipitate was filtered and extracted with methanol, hexanes, and chloroform. The trace Pd salts and unreacted monomers were removed by Soxhlet extraction with methanol. Further extraction with hexane removed oligomers and low molecular weight fractions from the polymers, and the soluble fraction was collected by extraction with chloroform.

Characterization. Gel permeation chromatography (GPC) was performed on a Waters 2690 separations module apparatus and a Waters 2487 dual λ absorbance detector with chloroform as the eluent (flow rate 1 mL/min, 35 °C, λ = 254 nm) and a series of three Styragel columns (10^4, 500, 100 Å; Polymer Standard Services). Toluene was the internal standard, and calibration based

on polystyrene standards was applied to determine molecular weights. ^{1}H NMR spectra of the polymer solutions in $CDCl_3$ were recorded on a Bruker Avance 500 MHz spectrometer. UV−vis−NIR spectra were measured on polymer solutions in anhydrous chloroform and polymer thin films cast onto a 22-mm square cover glass using a UV−vis−NIR spectrophotometer (Varian Cary 5000). Electrical conductivity measurements were performed by a standard spring-loaded pressure contact Signatone S-301-4 four-point probe, which was connected to a Hewlett-Packard 6632A system dc power supply, a Hewlett-Packard 3457 A multimeter (for voltage measurements), and a Keithley model 196 system DMM (for current measurements). Fluorescence measurements in anhydrous chloroform were carried out on a Photon Technologies International fluorimeter.

Cyclic Voltammetry. Cyclic voltammetry experiments were carried out on Autolab PGSTAT 100 using a three-electrode cell. Platinum wire was used as the counter electrode. The platinum stick electrode coated with a thin film layer of polymers was used as working electrode. Ag/Ag^+ electrode (Ag in a 0.01 mol/L $AgNO_3$) was used as the reference electrode, calibrated against the Fc/Fc^+ couple (0.09 V vs Ag/Ag^+) at the beginning of the experiment. An anhydrous and nitrogen-saturated solution of 0.1 M of tetrabutylammonium hexylfluorophosphate (n-Bu_4NPF_6) in acetonitrile was employed as the supporting electrolyte.

Out-of-Plane and In-Plane X-ray Diffraction. Out-of-plane and in-plane X-ray diffraction (XRD) scans of polymer thin films were performed on a Philips X'Pert Pro diffractometer. Copper radiation was used with a polycapillary lens. The Philips was operated at 45 kV and 40 mA. Incident crossed slits were 4 mm wide by 4 mm high. The Ψ tilt angle was 0° for out-of-plane scans and 88° for in-plane scans. The step size for all scans was 0.1° with a count time of 10 s/step, except for the range between 19 and 26° 2θ where a 40-s count time was used. Large size (2×2 cm^2) silicon wafers were used as XRD sample substrates; thin film samples for XRD analysis were prepared by drop-casting a 1 mg/mL solution in dry chloroform onto substrates treated with octyltrichlorosilane (OTS) under the same conditions as those used for FET devices.

Fabrication and Characterization of FET Devices. Organic field effect transistors were fabricated in the bottom gate, bottom contact configuration on heavily doped n-type Si substrates as the gate and a thermally grown 250-nm silicon dioxide as the dielectric layer (Silicon Quest, dry oxide). The source and drain electrodes were patterned using standard photolithography and were deposited on SiO_2 by sputter deposition of ~5 nm of titanium and 50 nm of gold. Before use, the devices were cleaned for 20 min by exposure to UV light in air (Novascan PSD-UVT) and heat (hot plate, 60−120 °C). The devices were surface-treated with OTS by immersion in a ~30 mM solution in anhydrous hexadecane at room temperature for 1−3 h. The devices were then cleaned by rinsing with HPLC-grade toluene and dried under nitrogen flow followed by vacuum for at least one hour. Polymer films were deposited in air by drop-casting 5 μL of a 1 mg/mL solution in dry chloroform and allowed to dry in a glass Petri dish saturated with chloroform. After film formation, the devices were further dried overnight in a desiccator under vacuum. Electrical measurements of the FETs were made under a flow of argon using an Agilent 4155C semiconductor parameter analyzer and a Micromanipulator S6 probe station. When measuring current−voltage curves and transfer curves, V_G was scanned from −80 to +40 V. The field effect mobilities were obtained from the transfer curves in the saturation regime at V_{DS} = −80 V. A line drawn through the linear part of an $I_{DS}^{1/2}$ vs V_G plot allowed extraction of threshold voltage and field effect mobilities using the square-law equation for the saturation regime. The average mobility was obtained from two or three transistors with channel length (L) ≥ 15 μm/polymer film and for at least eight different polymer films usually cast on different days.

Table 1. Number Average Molecular Weight (M_n), Polydispersity (M_w/M_n), and Polymerization Yield of the Copolymers

polymers	M_n[a] (kg/mol)	M_w/M_n[a]	yield (%)[b]
P1	30	1.8	62
P2	48	1.7	69
P3	47	1.7	68
P4	50	1.7	67
P5	41	2.1	92[c]
P6	32	1.7	55
P7	16	1.9	46

[a] Calculated from GPC (eluent: chloroform; polystyrene standards). [b] Yields were determined on the basis of the soluble fraction of the polymer in chloroform. [c] Yields were determined on the basis of the soluble fraction of the polymer in hexanes.

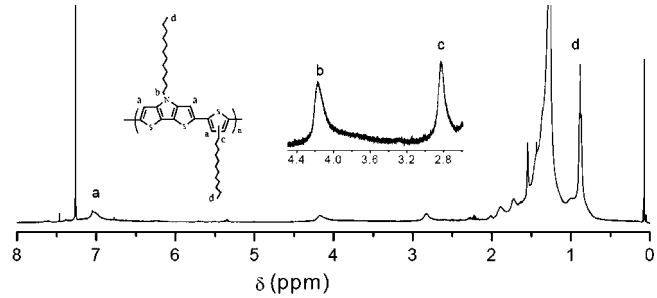

Figure 1. ^{1}H NMR spectra of P4.

Results and Discussion

Synthesis. *N*-Alkyl-2,6-bis(trimethylstannyl)dithieno[3,2-*b*:2'3'-*d*]pyrroles were prepared by first lithiating *N*-alkyl dithieno[3,2-*b*:2′,3′-*d*]pyrroles using 2.5 equiv of *t*-BuLi and then adding trimethyltin chloride to yield monomer **2** (Scheme 1). Any attempt to purify **2** by column chromatography failed, and NMR showed that **2** was pure enough to use directly in the polymerization via Stille cross-coupling (Scheme 1). Different 3-alkylthiophenes and 3,4-dialkylthiophene were copolymerized with DTP to study the effect of alkyl chain length and substitution pattern on polymer properties. Tail-to-tail (TT)-bialkylbithiophene (4,4′-didodecyl-2,2′-bithiophene) and HH-bialkylbithiophene (3,3′-dihexyl-2,2′-bithiophene) were also incorporated with DTP to investigate the effects of the DTP/TH ratio on the polymer and the different couplings. The results for each polymerization are summarized in Table 1. GPC data demonstrate that M_n of DTP-*co*-THs is between 16 and 50 kg/mol. These values are an order of magnitude higher than M_n of PDTPs.[17] Interestingly, the molecular weight of the polymers decreased from P4 to P7, probably because of the monomers' increased steric hindrance making them less reactive in the polymerization.

In addition to their high molecular weight, the novel DTP-*co*-THs showed excellent solubility in common organic solvents such as THF, chloroform, toluene, and chlorobenzene at room temperature. Additionally, they (except P5) exhibited good film-forming properties and can easily form uniform dark purple films by either drop-casting or spin-coating at room temperature.

The chemical structures of DTP-*co*-THs were confirmed by ^{1}H NMR spectroscopy, and the NMR spectrum of P4 is shown in Figure 1. The single peak at 4.2 ppm corresponds to the methylene (N−CH_2−) protons from DTP, and the peak at 2.8 ppm corresponds to α-methylene protons of 3-dodecylthiophene. The broad resonance at 7.0 ppm is assigned to the aromatic proton. On the basis of the relative areas of the peaks at 4.2

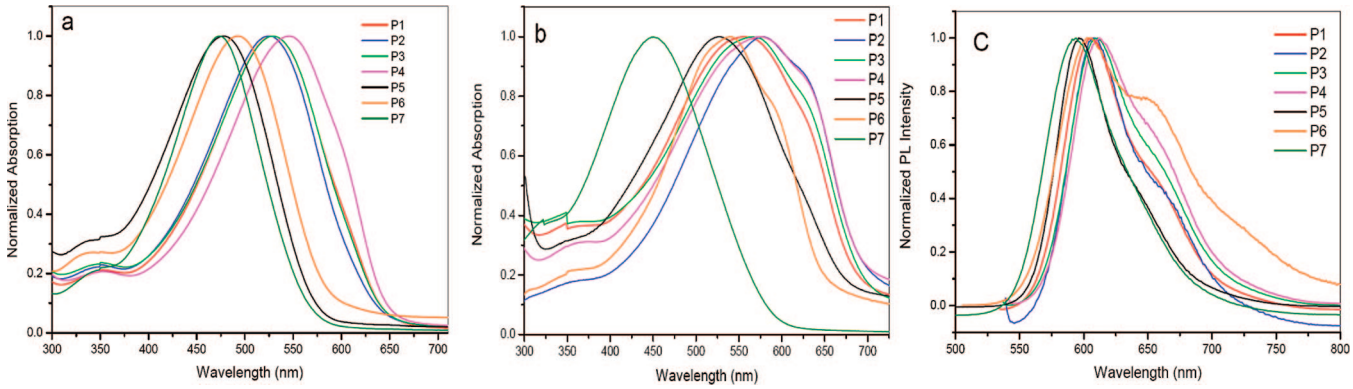

Figure 2. (a) Normalized absorption spectra of the polymer solutions in chloroform after being reduced with hydrazine hydrate. (b) Normalized absorptions of the polymer films drop-cast from dedoped chloroform solution. (c) Normalized PL spectra of polymer in chloroform solution.

Table 2. Optical Properties, Electrochemical Properties, and Conductivity of DTP-*co*-THs

polymers	λ_{max} (nm) solution	λ_{max} (nm) film	λ_{em} (nm) solution	Δ (nm)[b]	E_g (eV)[c]	E_{ox} (V vs Ag/Ag$^+$)/ HOMO (eV)[d]	conductivity (S/cm)[e]
rr-P3HT[a]	442	504			1.90	0.27/−4.98	160
P1	527	560	606	79	1.79	0.04/−4.75	67
P2	525	570	608	83	1.75	0.13/−4.84	95
P3	529	568	611	82	1.75	0.10/−4.81	82
P4	548	575	612	64	1.74	−0.03/−4.68	233
P5	478	535	596	118	1.81	0.25/−4.96	
P6	492	527	604	112	1.86	0.17/−4.88	68
P7	473	477	594	121	2.00	0.25/−4.96	15

[a] P3HT: Poly(3-hexylthiophene). [b] Stokes shift in solution, $\Delta = \lambda_{em} - \lambda_{abs}$. [c] Optical band gap. [d] All potentials are reported vs Fc/Fc$^+$ based on the assumption that the redox couple of Fc/Fc$^+$ is 4.8 eV relative to vacuum. [e] Maximum number.

and 2.8 ppm, the molar ratio of DTP and TH was determined to be 1:1, which is consistent with the proposed copolymer structure.

Optical Properties. In conjugated polymers, the extent of π conjugation can be predicted from the electronic spectra. The maximum absorption (λ_{max}) corresponds to a $\pi-\pi^*$ transition, and a large λ_{max} signifies a long effective conjugation length.[23] UV−vis spectra of the polymers were measured in dilute chloroform solution as well as in drop-cast films. Since neutral P1−P4 are readily oxidized in air, hydrazine hydrate was added to reduce these polymers immediately before the measurement. The spectra are shown in Figure 2, and the absorption data of the polymers are summarized in Table 2. Compared to that of *rr*-P3HT[3] and PDTPs,[17b] the λ_{max} values of DTP-*co*-THs (except for P7) were significantly red-shifted in both solution and solid state. As expected, λ_{max} also red-shifted as the ratio of the DTP units increased in the polymer backbone. For example, in the solid state, λ_{max} of regioirregular P4 with DTP/TH ratio of 1:1 was 48 nm red-shifted relative to that of regioregular P6 with DTP/TH ratio of 1:2. These results clearly indicate that the incorporation of a DTP fused ring into the polymer backbone led to a more planar structure and longer effective conjugation length.

P6, which consists of alternating DTP- and TT-coupled alkylthiophene units, exhibited a thin film λ_{max} at 527 nm. In sharp contrast, P7, which has HH-coupled alkylthiophene units, displayed a much shorter λ_{max} at 477 nm. This may be due to a dramatic decrease of conjugation caused by steric hindrance of the HH linkage between thiophene units. These results indicate that the effective conjugation length also depends on the twist angle of the polymer's backbone.

The effects of the alkyl chains on the optical properties were also investigated. However, there is no obvious influence on alkyl chain length. Interestingly, P4 with both dodecyl groups on DTP and thiophene units had the highest λ_{max} in both film and solution. Comparing P5 with P4, polymers with dialkylthiophene units showed smaller λ_{max} than those with monoalkylthiophene units (P1−P4) due to the steric repulsions.

The UV−vis absorption of P1−P4 in diluted chloroform solutions exhibited very broad absorptions with λ_{max} between 525 and 548 nm, whereas their thin films showed absorption with λ_{max} from 560 to 575 nm. The bathochromic shift found between the solutions and solid state spectra is due to enhanced interchain association in the solid state.[24] In contrast to those of *rr*-P3AT ($\Delta\lambda = 60-80$ nm),[3] this small bathochromic shift (~30 nm) strongly suggests that P1−P4 have relatively rigid structures and might have similar conformations in both solution and solid states.

The emission spectra of the polymers were measured in dilute chloroform solution ($<10^{-5}$ M) and are shown in Figure 2c. In solution, P1−P4 and P6 exhibit red emission with λ_{max} of 600−615 nm along with shoulders around 660 nm. These shoulders suggest better resolved vibronic structures, indicating higher ordered polymer structures,[25,26] which can also be supported by the small Stokes' shifts of P1−P4 and P6. In the case of solid state, only P7 was detected to exhibit fluorescence, which has a λ_{max} of 642 nm. This might be because P1−P6 have a relatively rigid structure that facilitates aggregation in the solid state, favors the interchain excitations, and hence quenches the fluorescence.[27] Suppressing the polymer aggregation by introducing the highly twisted HH-bialkythiophene unit in P7 enhanced the PL efficiency. P7 might be a useful material for LEDs.

The optical band gaps (E_g) of all polymers were determined from the UV−vis absorption onset.[28] The estimated band gaps are listed in Table 2. As can be seen, polymers P1−P6 have

(23) Shi, C.; Yao, Y.; Yang, Y.; Pei, Q. *J. Am. Chem. Soc.* **2006**, *128*, 8980.
(24) Politis, J. K.; Nemes, J. C.; Curtis, M. D. *J. Am. Chem. Soc.* **2001**, *123*, 2537.
(25) Pei, J.; Yu, W.; Huang, W.; Heeger, A. J. *Macromolecules* **2000**, *33*, 2462.
(26) Barta, P.; Cacialli, F.; Friend, R. H.; Zagórska, M. *J. Appl. Phys.* **1998**, *84*, 6279.
(27) Gigli, G.; Barbarella, G.; Favaretto, L.; Cacialli, F.; Cingolani, R. *Appl. Phys. Lett.* **1999**, *75*, 439.
(28) Bundgaard, E.; Krebs, F. *Macromolecules* **2006**, *39*, 2823.

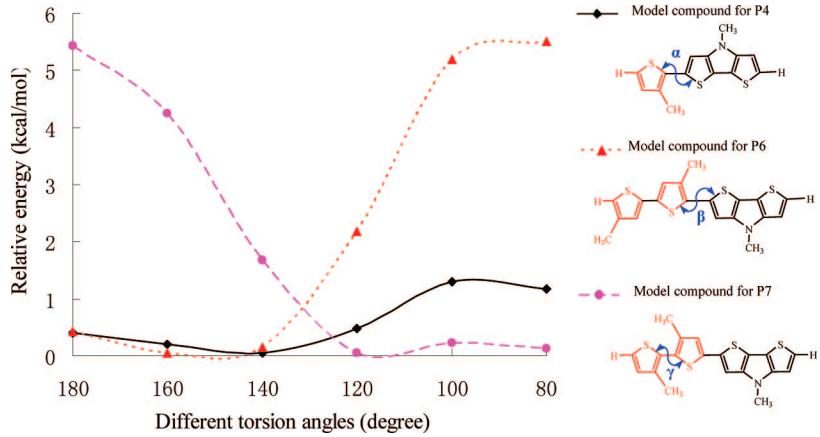

Figure 3. Calculated energies of P4, P6, and P7 representative at different torsion angles.

band gaps between 1.74 and 1.86 eV, which are smaller than *rr*-P3HT (1.90 eV). This low band gap can be due to the more coplanar structure of the polymer and the weak donor−acceptor effect of DTP and THs. Regioirregular P1−P4 have a 1:1 ratio of TH/DTP units in the backbone. They have the lowest band gaps between 1.74 and 1.79 eV among DTP-*co*-THs.

In summary, π conjugation is readily tunable either by changing the ratio of DTP/TH in the polymer or by introducing TT and HH coupling substituted bithiophene units.

Preferred Conformations. The polymer structure is affected by the thiophene substitution patterns on the DTP-*co*-THs backbone. This effect can be examined by calculating the energy from various conformation models for each linkage. Model compounds of P4, P6, and P7 containing methyl side groups (Figure 3) were designed for the calculations. First, the optimized energy geometries of each molecule were calculated using Hartree−Fock 3-21G basis set. The results revealed that all the adjacent rings prefer to be trans to each other. If the adjacent thiophene rings have a TT linkage or if the tail of the thiophene rings is linked with adjacent DTP rings, the two adjacent rings prefer trans coplanarity. In all other cases, the two adjacent rings twist in their minimum energy conformation. The energy of the different torsion angles (defined as dihedral angles α, β, and γ) of these twisted adjacent rings was then calculated using density functional theory at the B3LYP/6-31G* level. This allowed us to determine the minimum energy geometries and the energy barriers for adopting a planar conformation.

For model compounds P4 and P6, the minimum-energy geometries twisted with α of 160° and β of 140°, respectively (Figure 3). The calculated energy barrier for adopting a trans planar conformation is less than 0.2 kcal/mol. Because of the low energy barrier, the adjacent DTP and TH rings can display trans planarity. In contrast, the minimum energy geometry of model compound P7 is highly twisted at the HH linkage with dihedral angle γ of 120°. Up to 5.5 kcal/mol is required to adopt a trans coplanar conformation from this minimum energy geometry. Therefore, it may be unlikely for HH coupling thiophene rings to adopt planarity. This result indicates that the HH linkages in the polymer backbone decrease conjugation, increase the band gap, and inhibit intrachain charge transfer.[29] The calculations are in agreement with the reported calculations from McCullough et al.[3] and Matzger et al.[30] and support the optical, electronic, and conductivity results from the experiments.

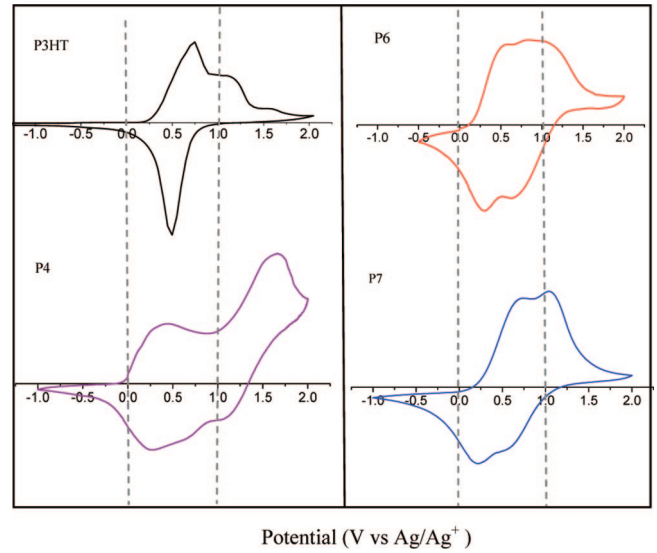

Figure 4. Cyclic voltammogram (current vs potential) of P4, P6, P7, and *rr*-P3HT at a scan rate of 100 mV s^{-1}.

Electrochemical Properties. The oxidation/reduction properties and electrochemical stability of the polymers are important for device design and control. To understand these properties and compare them to *rr*-P3HT, electrochemistry of the DTP-*co*-THs and *rr*-P3HT thin films coated on a Pt electrodes was investigated in 0.10 M tetrabutylammonium hexylfluorophosphate (n-Bu_4NPF_6) acetonitrile solutions by cyclic voltammetry at a scan rate of 100 mV s^{-1}.

All DTP-*co*-THs exhibited reversible or partial reversible oxidation (p-doping) processes. The cyclic voltammograms of *rr*-P3HT and representative DT-*co*-THs are shown in Figure 4. The onsets of oxidation (E_{ox}) of P4, P6, and P7 are −0.03, 0.17, and 0.25 V versus Ag/Ag^+, respectively, which is lower than *rr*-P3HT (0.27 V versus Ag/Ag^+). The relatively low oxidation potential may be caused by two factors. First, the introduction of electron-rich DTP rings lowers the polymers oxidation potential. Second, the incorporation of the rigid, fused DTP ring results in extensive π conjugation of the polymers, also lowering the oxidation potentials. The low oxidation potentials lead to very stable DTP-*co*-THs in oxidized states relative to P3HT. It can be noted that the introduction of HH-linked bialkylthiophene into DTP polymer (P7) increased the oxidation potentials as compared with the introduction of TT bialkylthiophene (P6) as

(29) McCullough, R. D. *Adv. Mater.* **1998**, *10*, 1.
(30) Zhang, X.; Köhler, M.; Matzger, A. J. *Macromolecules* **2004**, *37*, 6306.

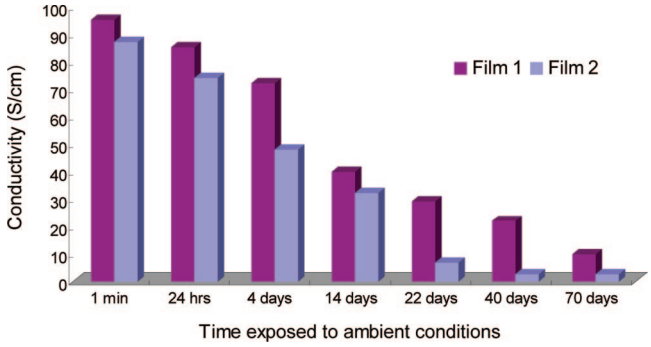

Figure 5. Time dependence of conductivity of iodine-doped films (films 1 and 2) of P2 after exposure to ambient conditions.

a result of decreased conjugation length, all consistent with the structure calculation.

HOMO levels of the polymers were calculated from the onset of the oxidation peak (E_{ox}), on the basis of the assumption that the HOMO of ferrocene/ferrocenium (Fc/Fc^+) is at 4.8 eV from vacuum.[31] LUMO levels were estimated from the HOMO values and the optical band gaps. The electrochemical properties are summarized in Table 2. The calculated HOMO energy levels of DTP-*co*-THs are between −4.68 and −4.96 eV, and the LUMO energy levels are between −2.94 and −3.15 eV.

Electrical Conductivity. The samples for electrical conductivity measurements were prepared by drop-casting the polymer from chloroform solutions at room temperature. The films were doped with iodine for two hours. The electrical conductivities were measured by the four-point probe technique, and film thickness was measured by profilometry. Conductivities were calculated according to eq 1,[32] and are reported in Table 2.

$$\sigma = \frac{1}{4.53Rl} \tag{1}$$

where R is the resistance ($R = V/I$) and l is the thickness of the film.

Except for P5, DTP-*co*-THs form very uniform films and show high conductivity in the range of 15−233 S/cm. P4 exhibited the highest average electrical conductivities of 160 S/cm and maximum conductivities of 233 S/cm with 0.4-μm thickness. Furthermore, it was found that iodine-doped P1−P4 were quite stable under ambient conditions and could retain high conductivities over several weeks. For example, the conductivity of P2 was 95 S/cm after being doped with iodine for 2 h. Then after exposure to ambient conditions for three months, it still retained a value of 10 S/cm (Figure 5). In contrast, the conductivities of iodine-doped P3HT films significantly decrease within a few hours to 0.1 S/cm. The high conductivity as well as the excellent stability in doped states makes P1−P4 promising materials for electronic applications.

Microstructure Characterization. Regioirregular P4 and regioregular P6 were selected as representatives for studying the microstructures because of their different regioregularity and high conductivity. The microstructures of P4 and P6 thin films were investigated by XRD, and the surface morphologies of thin films were studied by tapping-mode atomic force microscopy.

Thin films of P4 and P6 were prepared by drop-casting from solvent (chloroform) onto OTS-treated silicon substrates. Before thin film deposition, the solutions were filtered through a 0.2-μm-pore-sized poly(tetrafluoroethylene) syringe filter. To facilitate equilibration of nanostructures, deposition was carried out under saturated solvent vapor by placing the substrate in a covered Petri dish partially filled with the solvent.

Out-of-plane and in-plane $\theta-2\theta$ scattering profiles of P4 thin films on OTS-treated SiO_2/Si substrate are shown in Figure 6. Samples as-cast appeared to be highly disordered, and the only distinguishable scattering feature was the weak peak centered at $2\theta = 4.5°$ ($q = 0.28$ Å^{-1}), which appeared to be stronger for in-plane scattering. In analogy with *rr*-P3HT, this scattering feature could be assigned to molecular sheets of polymer backbones with the intersheet spacing of ∼22.4 Å. Interestingly, whereas the molecular sheets in thin films of *rr*-P3HT tend to be aligned in the plane of the film (i.e., parallel to the substrate), here they appeared to be more isotropic, with some preference of the orientation perpendicular to the substrate (cf. more pronounced in-plane scattering). After being thermally annealed at 120 °C for 30 min, the feature corresponding to lamellar organization became more pronounced (Figure 6, red traces); the preferential orientation of lamellae perpendicular to the surface was now also more apparent. Annealing also led to the appearance of a peak in the out-of-plane scattering patterns, centered at $2\theta = 24.3°$ ($q = 1.74$ Å^{-1}, spacing of 3.6 Å). This feature can be viewed as an indication of the presence of π stacking, with the π stacking plane parallel to the film substrate. The microstructure changes before and after annealing can be clearly seen from the proposed model in Figure 7. It should be noted that the observed orientation of lamellar sheets and π stacking is in contrast with the in-plane lamellar orientation commonly observed in *rr*-P3HT.

Initially disordered state of P4 and the development of some ordering with annealing were also evident in AFM height images of this sample (Figure 8). Surfaces of as-cast P4 had barely discernible granular morphology, similar to one observed for glassy polymers (Figure 8a). In contrast, the images of the samples subjected to 30 min of vacuum annealing at 120 °C followed by slow cooling to room temperature (Figure 8b) revealed the presence of distinct, uniform, cigar-shaped features, most likely corresponding to P4 microcrystallines.

Increase of long-range order with annealing was also evident in XRD patterns of thin films of P6 on OTS-treated SiO_2/Si substrates (Figure 9). As with P6, the only distinguishable feature in the diffractograms of as-cast samples (black traces) was the low-angle peak indicating the presence of randomly ordered lamellar structure with the d spacing of ∼24.2 Å. Upon annealing, the intensity of the out-of-plane peak corresponding to this feature increased dramatically (its second-order component also became stronger), and the d spacing decreased to ∼21.8 Å, indicating tighter packing. No evidence of π stacking was observed for the P6 sample, even after annealing. In contrast with P4, for this sample it would be difficult to point to the similar correspondence between XRD patterns and AFM data. To the contrary, the crisscrossing straight nanofibrils observed in the AFM images of as-cast P6 films (Figure 10a) were no longer discernible in the images of annealed samples (Figure 10b).

Field Effect Mobility Measurements. The field effect mobilities of P4, P6, and P7 were measured using FETs fabricated as described in the Experimental Section. The field effect mobilities were measured under flowing argon and calculated from transfer curves taken in the saturation regime. Figure 11 shows typical output and transfer curves for P6 without postdeposition thermal

(31) Pommerehne, J.; Vestweber, H.; Guss, W.; Mahrt, R.; Bassler, H.; Porsch, M. *Adv. Mater.* **1995**, *7*, 551.
(32) Iovu, M. C.; Jeffries-EL, M.; Sheina, E. E.; Cooper, J. R.; McCullough, R. D. *Polymer* **2005**, *46*, 8582.

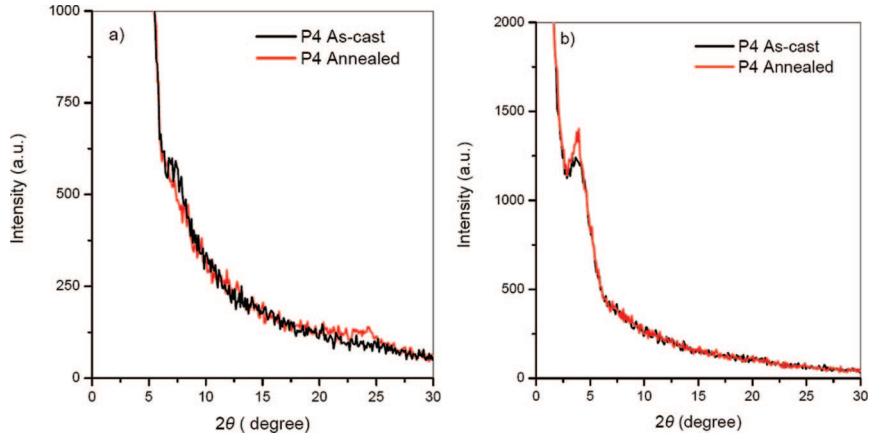

Figure 6. XRD profile of P4 thin films on OTS-treated SiO_2/Si substrate as-cast (black trace) and after annealing at 120 °C for 30 min (red trace). (a) Out-of-plane XRD profile. (b) In-plane XRD profile.

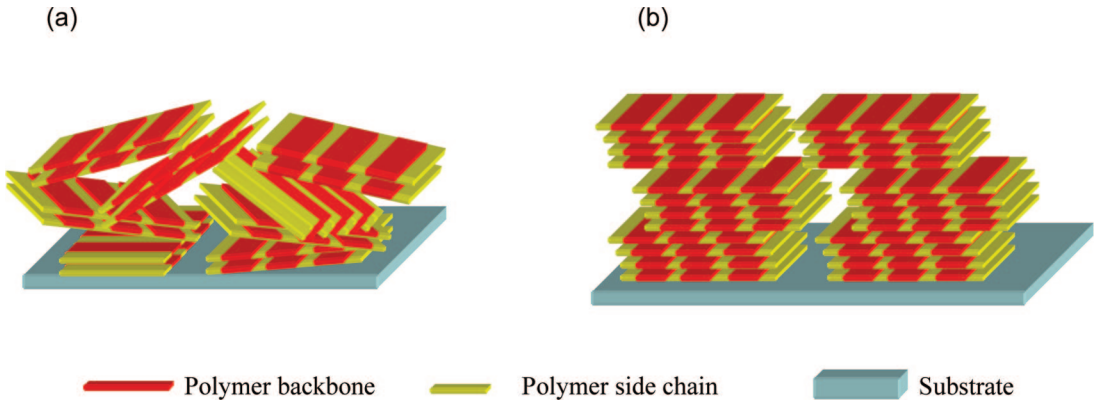

Figure 7. Scheme of molecular packing of P4 (a) as-cast and (b) after annealing at 120 °C for 30 min.

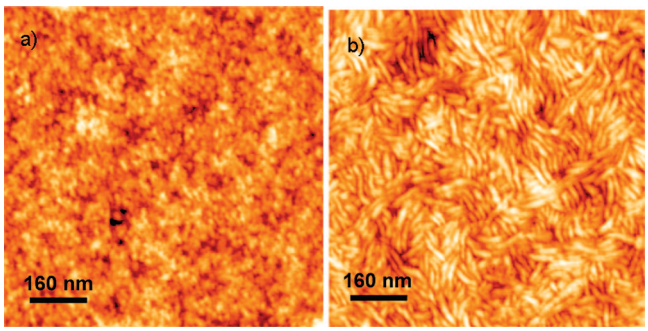

Figure 8. Tapping-mode AFM height images of P4 drop-cast on OTS-treated SiO_2/Si surfaces (a) as-cast and (b) annealed at 120 °C for 30 min then cooled to room temperature in a vacuum.

annealing. The devices exhibited good FET behavior and no noticeable contact resistance. In all cases, the mobility data were obtained from at least eight different films using transistors with channel lengths from 15 to 40 μm to avoid short channel effects. The distributions of the mobility measurements for each polymer were shown in a box-and-whisker plot, which indicates 25, 50, and 75% of the data is below or at that point (Figure 12). For P4 and P7 as-cast and annealed samples, 16 data points are included in each case. As for P6, 25 data points are included in both as-cast samples and annealed samples. The overall summaries of transistor performances are provided in Table 3.

Among all the samples, as-cast P6 exhibited the best field effect performance with the highest mobility of 0.21 $cm^2\ V^{-1}\ s^{-1}$ and an average mobility of 0.13 $cm^2\ V^{-1}\ s^{-1}$. Interestingly, these values are *higher* than the highest reported field effect mobilities of *rr*-P3HT[33] and are *highly consistent* and *reproducible* from batch to batch as evident from a box-and-whisker plot shown in Figure 12. Comparable mobility was also observed for sample P4, whereas the mobility in sample P7 was on average more than 1 order of magnitude lower, which is not surprising, given its structure which did not allow extensive conjugation.

Interestingly, after thermal annealing at 120 °C for 30 min, the mobilities of all the samples *decreased*, in some cases by as much as 1 order of magnitude. This trend might appear as rather unusual, especially given the just discussed structural evidence that in all cases annealing resulted in some improvement of the overall degree of long-range ordering (Figures 6 and 9). Behavior observed here appears to contradict the well-known correlation between the presence of highly ordered microcrystalline structures and high FET performance of systems such as *rr*-P3HT, PBTTT,[6b,34] and PQT.[1c,35] Polymers studied here clearly do not belong to this category. The highest mobilities were observed for as-cast samples P6 and P4, which according to X-ray diffraction were highly isotropic and exhibited weak scattering features corresponding to lamellar ordering and no evidence of $\pi-\pi$ stacking. This apparent

(33) Chang, J.; Sun, B.; Breiby, D. W.; Nielsen, M. M.; Sölling, T. I.; Giles, M.; McCulloch, I.; Sirringhaus, H. *Chem. Mater.* **2004**, *23*, 4772.
(34) Chabinyc, M. L.; Toney, M. F.; Kline, R. J.; McCulloch, I.; Heeney, M. *J. Am. Chem. Soc.* **2007**, *129*, 3226.
(35) (a) Ong, B. S.; Wu, Y.; Liu, P.; Gardner, S. *Adv. Mater.* **2005**, *17*, 1141. (b) Zhao, N.; Botton, G. A.; Zhu, S.; Duft, A.; Ong, B. S.; Wu, Y.; Liu, P. *Macromolecules* **2004**, *37*, 8307.

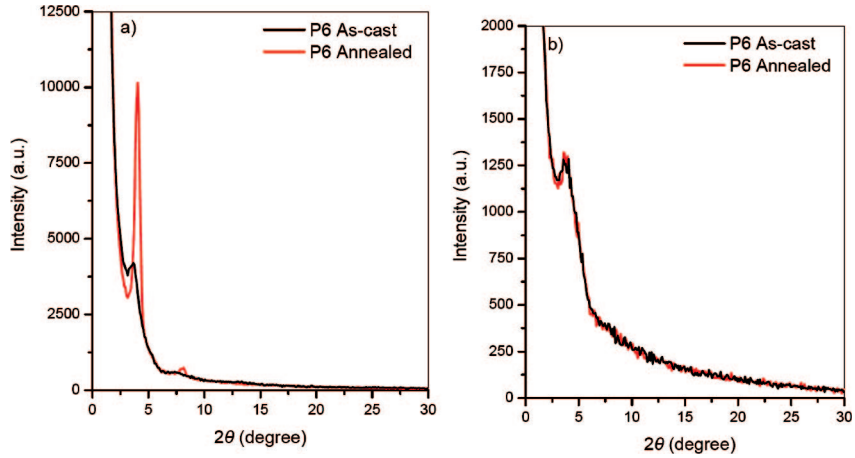

Figure 9. XRD profile of P6 on OTS-treated SiO_2/Si substrate as-cast (black trace) and after annealing at 120 °C (red trace). (a) Out-of-plane XRD profile. (b) In-plane XRD profile.

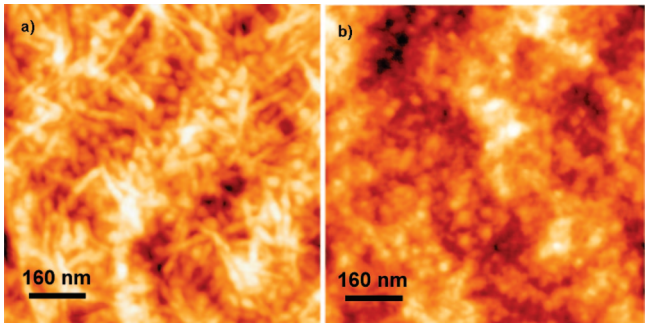

Figure 10. Tapping-mode AFM height images of P6 drop-cast on OTS-treated SiO_2/Si surfaces (a) as-cast and (b) annealed at 120 °C for 30 min then cooled to room temperature in a vacuum.

contradiction can be understood given the results of the Hartree−Fock calculation using the 3-21G basis set, which showed that the spacing between the neighboring side chains in P4 and P6 is much larger than one observed for *rr*-P3HT. In condensed phase, this less-dense placement of side chains along the backbone evidently weakens the driving force for the formation of well-defined lamellar structures, at the same time opening the opportunities for the conjugate backbones to engage in closer contacts, facilitating the interchain charge hopping in all directions. As a result, these isotropic, poorly ordered samples exhibit quite high values of carrier mobility. Since P4 and P6 are readily soluble in common organic solvent at room temperature, easily form uniform films, show high field effect mobilities without any required complex processing, this behavior makes them attractive candidates for OFET mass manufacturing process using common printing techniques (e.g., inkjet printing).

One is still left with the question why the development of microcrystalline ordering upon annealing proved to be detrimental for transport. In the case of sample P4, which exhibited a more pronounced drop of mobility, this can be understood by realizing that $\pi-\pi$ stacking developed in the direction perpendicular to the substrate (Figure 6), presumably because of the tendency of flat fused DTP rings to lay parallel to the substrate or thin film surface. This in turn created the situation in which charges traveling through the conductive channel had to move from one crystallite to another through intervening layers of insulating alkyl chains, thus exhibiting lower mobility. The situation is not so clear in the case of sample P6, in which annealing resulted in the development of lamellae parallel to the substrate (Figure 9), which normally should lead to the improvement of transport conditions. One could argue though that the observed *moderate* decrease of mobility points to the fact that, in the net balance, the development of better lamellar order does not offset the loss of closer backbone-to-backbone

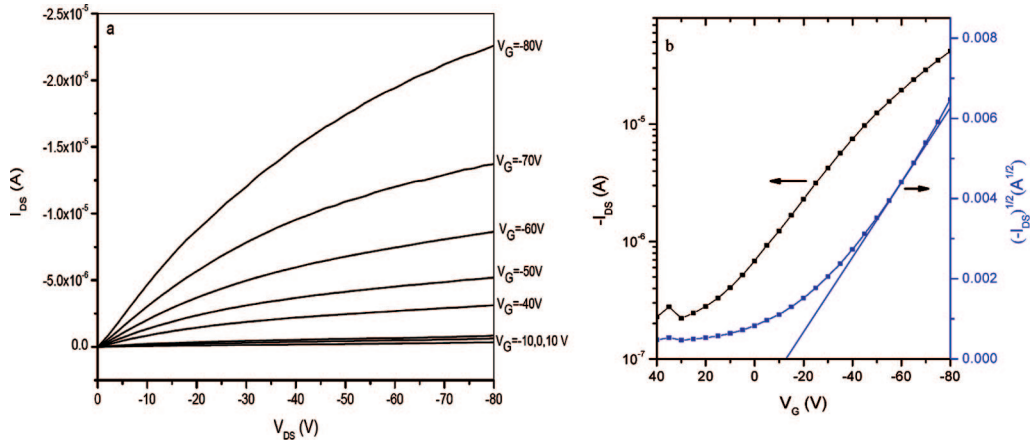

Figure 11. Current−voltage characteristics of P6 on OTS-8 treated SiO_2 devices. (a) Output curves at different gate voltages. (b) Transfer curve at $V_{DS} = -80$ V. (The extracted mobility was 0.21 $cm^2\ V^{-1}\ s^{-1}$. The channel length was 30 μm, and the channel width was 250 μm.)

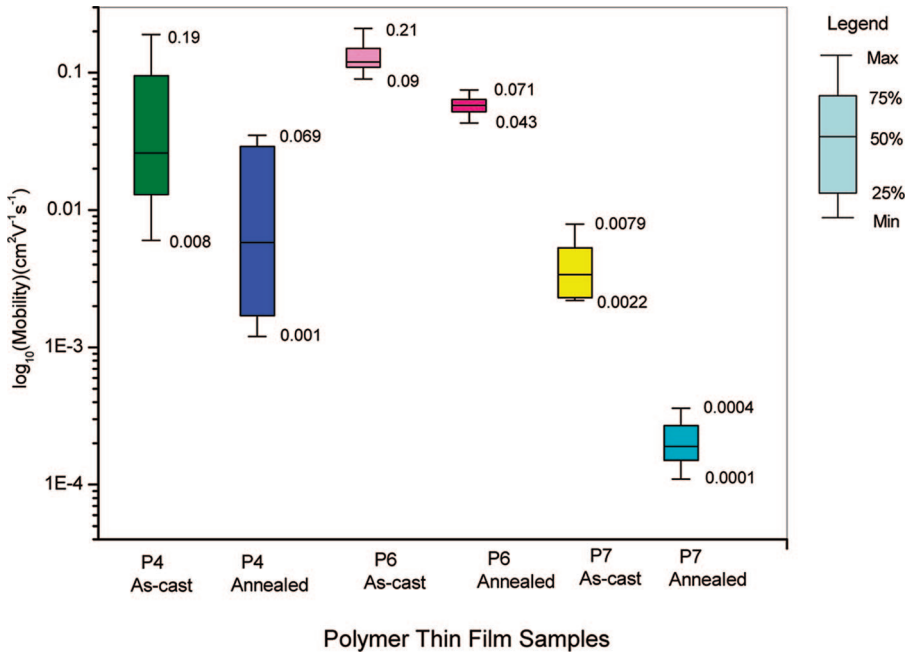

Figure 12. Box-and-whisker plot of field effect mobilities of P4, P6, and P7 as-cast and after annealing.

Table 3. Average Field Effect Transistor Parameters (See Also Figure 12)

polymer	condition	μ (cm^2 V^{-1} s^{-1}) (average)	on/off ratio	V_t (V)
P4	as-cast	0.026	4	60
	annealed	0.0058	20	50
P6	as-cast	0.13	120	−21
	annealed	0.058	1500	−14
P7	as-cast	0.0035	140	−23
	annealed	0.00019	150	−22

contacts. It should be also noted that in the case of this sample there was no evidence of appreciable $\pi-\pi$ stacking, even after annealing.

While disordered samples P4 and P6 exhibited good charge carrier mobilities, they had one potential drawback, low FET on/off ratios, resulting most likely from their low oxidation potentials (Figure 4).[36] This, however, could be improved by more extensive purification and by dedoping the polymers with common reducing agents.

Conclusions

In summary, we successfully synthesized a new class of DTP-based copolymers with high molecular weight and excellent solubility. Copolymers with different thiophene/DTP ratios and differently substituted alkyl side chains exhibited many desirable properties, such as low band gap, high stability in oxidized state, and, with the exception of head-to-head systems, high conductivity and carrier mobility. Interestingly, in all instances carrier mobilities determined from FET characteristics were higher for as-cast, poorly ordered samples, rather than for more ordered annealed ones. This atypical behavior has been tentatively ascribed to enhanced backbone-to-backbone contacts in less ordered systems (presumably facilitated by sparse placement of alkyl side chains), and thus more effective interchain hopping. With this regard, these materials appear to confirm that disordered, isotropic systems should exhibit enhanced performance. Given this and their excellent solubility, they could be good candidates for low-cost plastic electronics, fabricated using processes inherently leading to more disordered structures (e.g., inkjet printing). Of particular interest when it comes to the applications of these materials in FETs, OPVs, and OLEDs is the demonstrated possibility to tailor their π conjugation by the introduction of a fused ring system and stereochemistry.

Acknowledgment. We are grateful to Dr. Itaru Osaka and Dr. Sarada Mishra for their help in this work. Financial support was provided by the National Science Foundation (CHE0415369).

JA803077V

(36) Huisman, B.; Valeton, J. J. P.; Nijssen, W.; Lub, J.; Hoeve, W. *Adv. Mater.* **2003**, *15*, 2002.